ACS MATERIALS LETTERS

www.acsmaterialsletters.org

LETTER

High Breakdown Current Density in Monolayer $Nb_4C_3T_x$ MXene

Alexey Lipatov, Michael J. Loes, Nataliia S. Vorobeva, Saman Bagheri, Jehad Abourahma, Hanying Chen, Xia Hong, Yury Gogotsi, and Alexander Sinitskii*

Cite This: *ACS Materials Lett.* 2021, 3, 1088–1094

Read Online

ACCESS | Metrics & More | Article Recommendations | Supporting Information

ABSTRACT: MXenes are an emerging family of transition-metal carbides, nitrides, and carbonitrides that are promising for a variety of applications, including energy storage, gas sensors, and electromagnetic interference shielding. A recent report on a very high breakdown current density of ~1.2×10^8 A cm^{-2} in $Ti_3C_2T_x$ further extended the list of potential applications of MXenes to miniaturized on-chip interconnects. In this study, we investigated another promising member of the MXene family, $Nb_4C_3T_x$, and found that it also has a very high breakdown current density of ~1.1×10^8 A cm^{-2}, which is comparable to that of $Ti_3C_2T_x$ and other highly conductive two-dimensional materials, such as graphene. The measurements were performed on electronic devices based on individual monolayer flakes of $Nb_4C_3T_x$, which were tested at gradually increasing voltages until the electrical breakdown was observed. The morphology of $Nb_4C_3T_x$ devices after the breakdown was studied by microscopic techniques. The high breakdown current densities of $Ti_3C_2T_x$ and $Nb_4C_3T_x$ suggest that other members of the large MXene family likely possess this property and could be employed in applications utilizing their high current-carrying capacity.

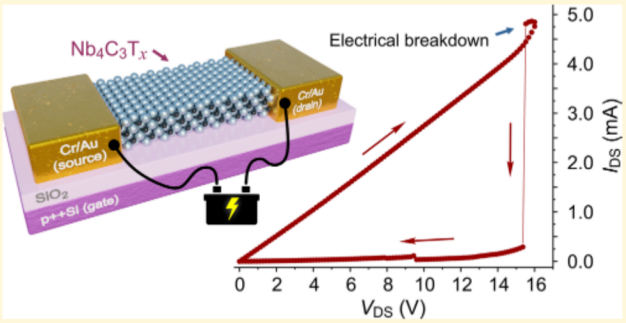

There is a growing interest in the synthesis, properties, and emerging applications of two-dimensional (2D) transition-metal carbides, nitrides, and carbonitrides, collectively known as MXenes.[1,2] These materials have a general formula $M_{n+1}X_nT_x$, where M is a transition metal, such as Ti, Nb, V, Ta, etc., X is carbon and/or nitrogen, T_x represents surface functional groups, and n = 1, 2, 3, or 4. MXene sheets are synthesized by selective etching of layers of an "A" element, such as Al or Si, from bulk crystals of layered MAX phases with a general formula $M_{n+1}AX_n$.[1] Dozens of MAX phases have been reported,[3] and in recent years, many of them have been subjected to the A-element etching, resulting in over 30 experimentally demonstrated MXene compositions, including $Ti_3C_2T_x$,[4] $Nb_4C_3T_x$,[5] $Mo_4VC_4T_x$,[6] and many others.[1,2]

Most experimental research so far has been focused on $Ti_3C_2T_x$,[1] which is the first discovered MXene material.[4] $Ti_3C_2T_x$ has exceptional electronic and mechanical properties,[7,8] which justify its promise for a large variety of applications ranging from energy storage[9,10] and photovoltaics[11] to electronic and photonic devices,[12] gas sensors[13,14] and electromagnetic interference shielding.[15] A recent study demonstrated that $Ti_3C_2T_x$ MXene also has a very high breakdown current density of ~ 1.2×10^8 A cm^{-2},[16] which extends the list of potential applications of MXenes to miniaturized on-chip interconnects in integrated circuits. Considering that this is currently the only study of breakdown current density in MXenes, it is unclear whether this high reported value is unique for $Ti_3C_2T_x$ or if some other members of the large MXene family possess similar or even better characteristics.

In this study, we investigated the breakdown current density in monolayer $Nb_4C_3T_x$ MXene (see the inset in Figure 1a).[5] While $Ti_3C_2T_x$ had been the most popular MXene material so far,[1] niobium carbides also received considerable attention as electrodes for Li ion batteries[17−19] and supercapacitors,[20] catalyst supports,[21] free-radical scavengers,[22] phototherapeutic cancer treatments,[23] and superconductors.[24] The choice of $Nb_4C_3T_x$ for this study was further justified by the availability of the synthetic procedure enabling large (a few micrometers in size) well-exfoliated MXene flakes[25] that are necessary for

Received: June 1, 2021
Accepted: June 15, 2021
Published: June 28, 2021

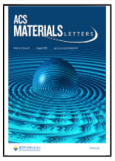

Downloaded via UNIV OF NEBRASKA LINCOLN on December 3, 2021 at 17:29:16 (UTC).
See https://pubs.acs.org/sharingguidelines for options on how to legitimately share published articles.

ACS Publications © 2021 American Chemical Society

https://doi.org/10.1021/acsmaterialslett.1c00324
ACS Materials Lett. 2021, 3, 1088−1094

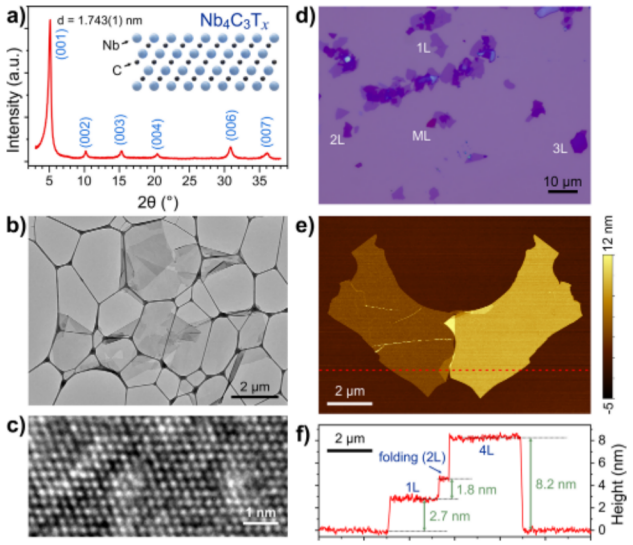

Figure 1. Characterization of the $Nb_4C_3T_x$ flakes. (a) XRD pattern of a $Nb_4C_3T_x$ film. The side view of a $Nb_4C_3T_x$ MXene monolayer is shown in the inset; the blue spheres represent Nb; the black spheres represent C; the surface functional groups (T_x) are omitted. (b) TEM image of $Nb_4C_3T_x$ flakes on a lacey carbon grid. (c) HRTEM image of a $Nb_4C_3T_x$ flake. (d) Optical image of monolayer (1L), bilayer (2L), trilayer (3L), and multilayer (ML) $Nb_4C_3T_x$ flakes on a Si/SiO_2 substrate. (e) AFM image of a multilayer $Nb_4C_3T_x$ flake next to a monolayer flake exfoliated from it. (f) Height profile measured along the red dashed line in the AFM image shown in panel (e).

nanofabrication of single-flake devices and their electrical measurements.[26]

The synthesis of $Nb_4C_3T_x$ MXene is described in our previous study[25] and summarized in the Supporting Information (SI). In brief, the synthetic procedure is based on the HF etching of Nb_4AlC_3 MAX phase[5] and delamination of the resulting $Nb_4C_3T_x$ using tetramethylammonium hydroxide (TMAOH). The procedure results in well-exfoliated $Nb_4C_3T_x$ MXene material with a large fraction of few-micrometer-sized flakes that could be conveniently used for device fabrication.[25] An aqueous solution of $Nb_4C_3T_x$ MXene was drop-casted on a substrate and dried to form a thick film that was analyzed by X-ray diffraction (XRD). The measurement was performed using a Rigaku Smart Lab powder diffractometer with Ni-filtered Cu Kα radiation. The XRD pattern shown in Figure 1a reveals a series of equidistantly spaced (00l) peaks ranging from (001) to (007), indicating a layered structure of stacked MXene flakes. The interplanar distance extracted from the XRD pattern of a $Nb_4C_3T_x$ MXene film is ~1.743 nm, which is consistent with the previous measurements.[25] According to the results of X-ray photoelectron spectroscopy (XPS), the $Nb_4C_3T_x$ MXene synthesized by the described HF etching route had a mixed O/F termination (see Figure S1 and its discussion in the SI).

The high quality of the $Nb_4C_3T_x$ flakes used for the device fabrication was confirmed by transmission electron microscopy (TEM). Figure 1b shows uniform $Nb_4C_3T_x$ flakes deposited on a lacey carbon TEM grid that are several micrometers in size. High-resolution transmission electron microscopy (HRTEM) of these flakes revealed the perfect hexagonal arrangement of the Nb atoms (Figure 1c). TEM was performed using a FEI Tecnai Osiris scanning transmission electron microscope at an accelerating voltage of 200 kV.

A droplet of an aqueous suspension of $Nb_4C_3T_x$ flakes was placed on a p-type silicon substrate covered with a 300-nm-thick layer of SiO_2 and dried in air. Individual MXene flakes with different thicknesses can be identified by optical microscopy according to their optical contrast (Figure 1d). The thickness of the flakes was investigated by atomic force microscopy (AFM), which was performed using a Bruker Dimension Icon AFM system operated in the PeakForce tapping mode. Figure 1e shows an AFM image of a few-layer $Nb_4C_3T_x$ flake along with a monolayer flake of exactly the same shape. The shapes of these flakes suggest that they originated from the same Nb_4AlC_3 crystallite. The AFM height profile analysis shown in Figure 1f confirms our previous findings that the thickness of a monolayer $Nb_4C_3T_x$ on Si/SiO_2 is ~2.7 nm, which is larger than its nominal thickness due to the presence of molecular adsorbates, such as water molecules, that are trapped between the substrate and the flake.[25] As we extensively discussed in our previous work,[25] $Nb_4C_3T_x$ monolayers that are measured by AFM on top of other $Nb_4C_3T_x$ flakes have a smaller thickness of ~1.8 nm (see the folded region in Figures 1e and 1f), which is similar to the value obtained by the XRD analysis (1.74 nm). Given that, for a multilayer flake, the bottom layer lying directly on Si/SiO_2 has a thickness of 2.7 nm and each subsequent layer adds ~1.8 nm to the overall thickness, we conclude that the thicker flake in Figure 1e consists of four $Nb_4C_3T_x$ monolayers (2.7 nm + (3 × 1.8 nm) = 8.1 nm).[25]

Several individual MXene flakes were identified by optical microscopy and used for patterning field-effect transistor (FET) devices by electron-beam lithography as described in our previous works.[7,25] The scheme of a typical MXene device used in this study is presented in Figure 2a. It shows a $Nb_4C_3T_x$ flake bridging Cr (5 nm)/Au (20 nm) source (S) and drain (D) electrodes on a Si/SiO_2 substrate; the conductive p-type Si layer served as the global back gate (G) electrode. Figure 2b shows a scanning electron microscopy (SEM) image of a representative device based on a bilayer $Nb_4C_3T_x$ flake; the Cr/Au electrodes are highlighted in yellow for clarity. SEM was performed using a Zeiss Supra 40 field-emission SEM system at an accelerating voltage of 5 kV.

The room-temperature electrical measurements of $Nb_4C_3T_x$ devices were performed under vacuum in a Lake Shore TTPX probe station at the base pressure of ~2×10^{-6} Torr, using an Agilent 4155C semiconductor parameter analyzer. Prior to the measurements, the devices were kept under vacuum for at least 2 days to minimize the effect of surface adsorbates.[27] The I_{DS}–V_{DS} dependences at three different gate voltages (−40, 0, and 40 V) for the device shown in Figure 2b are presented in Figure 2c. The linearity of the I_{DS}–V_{DS} dependences is indicative of Ohmic contacts between the MXene channel and the electrodes, which is consistent with the previously reported results of four-terminal electrical measurements of devices based on $Nb_4C_3T_x$ flakes with Cr/Au electrodes.[25] The superimposed I_{DS}–V_{DS} dependences measured at different V_G (Figure 2c) demonstrate the weak effect of gate voltage on the electrical conductivity of the device. The sheet resistances for the devices were calculated from the I_{DS}–V_{DS} curves measured at V_G = 0 and the flake dimensions. The bilayer $Nb_4C_3T_x$ device shown in Figure 2b has a sheet resistance of 3690 Ω $\square^{-1}$. MXene resistivity can then be calculated by dividing the sheet resistance by the flake thickness, which, for

https://doi.org/10.1021/acsmaterialslett.1c00324
ACS Materials Lett. 2021, 3, 1088−1094

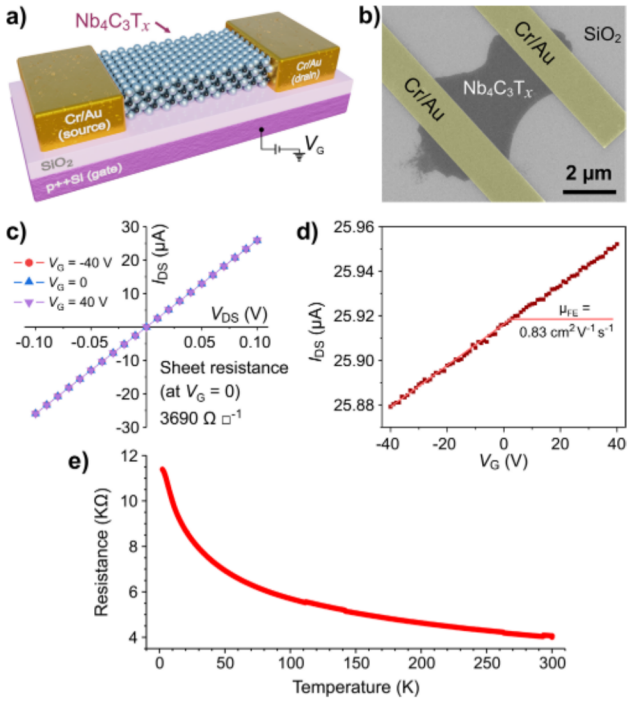

Figure 2. Electronic properties of $Nb_4C_3T_x$ flakes. (a) Scheme of a two-terminal device based on an individual $Nb_4C_3T_x$ flake. (b) SEM image of a representative device based on a bilayer $Nb_4C_3T_x$ flake. The electrodes are colored in yellow for clarity. (c) I_{DS}−V_{DS} dependences for the $Nb_4C_3T_x$ device shown in panel (b) measured at the gate voltages of −40, 0, and 40 V. (d) I_{DS}−V_G dependence for the same device measured at V_{DS} = 0.1 V. (e) Temperature dependence of resistance of the bilayer $Nb_4C_3T_x$ FET shown in panel (b).

bilayer $Nb_4C_3T_x$, can be estimated to be ∼2.52 nm.[25] The resulting resistivity for the MXene device shown in Figure 2b is 9.3 μΩ m and the corresponding conductivity is 1075 S cm^{-1}, both of which are in agreement with the previously published data for bilayer $Nb_4C_3T_x$ flakes.[25] Figure 2d shows the transfer characteristics for the same device measured at V_{DS} = 0.1 V in the V_G range from −40 V to +40 V. The I_{DS}−V_G dependence is linear and similar to our previous reports for MXene materials.[7,25] The positive slope of the I_{DS}−V_G dependence is indicative of the *n*-type transport. Field-effect mobilities (μ_{FE}) were extracted from the transfer characteristics using the formula $\mu_{FE} = C_d^{-1} \times \partial\rho^{-1}/\partial V_G$, where C_d is the capacitance of a 300-nm-thick SiO_2 dielectric layer and ρ is the resistivity of a $Nb_4C_3T_x$ device channel. For the bilayer $Nb_4C_3T_x$ device shown in Figure 2b, the calculated field-effect mobility is μ_{FE} = 0.83 cm^2 V^{-1} s^{-1}, which is larger than for typical monolayer $Nb_4C_3T_x$ flakes (∼0.49 cm^2 V^{-1} s^{-1}).[25]

Temperature-dependent resistance measurements were performed in a Quantum Design physical property measurement system (PPMS). Figure 2e shows the temperature dependence of resistance for the same bilayer $Nb_4C_3T_x$ MXene device (Figure 2b) in the temperature range from 2 K to 300 K. The resistance increases with decreasing temperature, which is in agreement with the previous reports on $Nb_4C_3T_x$ films[28] and individual flakes,[25] as well as several other MXenes.[29,30] Interestingly, a recent study demonstrated superconductivity above 4.2 K in Nb_2CT_x MXene with certain functional groups T, such as chlorine (Nb_2CCl_2 with a critical temperature (T_c) of ∼6.0 K), sulfur (Nb_2CS_2, $T_c \approx$ 6.4 K), and selenium (Nb_2CSe_2, $T_c \approx$ 4.5 K).[24] In contrast, the HF-etched Nb_2CT_x MXene with a mixed O/F termination did not exhibit superconductivity in the same temperature range from 2 K to 300 K.[24] The $Nb_4C_3T_x$ MXene flakes that were also produced in this work by the HF etching route had a mixed O/F surface termination[20,25] (see the results of the XPS analysis in Figure S1 in the SI) and did not exhibit superconducting properties at temperatures above 2 K (Figure 2e), which is consistent with the results reported for the HF-etched Nb_2CT_x.[24] However, these studies collectively suggest that superconductivity in $Nb_4C_3T_x$ MXene may be achieved by a precise control of surface functionalities, which could be a promising topic for future studies.

Figure 3 shows a series of I_{DS}−V_{DS} dependences that illustrate the current annealing and electrical breakdown in a representative monolayer $Nb_4C_3T_x$ FET. The microscopic images of this device can be seen in Figure 4. The measurements were performed at V_G = 0, and each I_{DS}−V_{DS} curve includes a forward V_{DS} scan from 0 to a certain value of $V_{DS,max}$ and a reverse scan back to 0. Figure 3a shows that when the drain-source voltage was scanned from 0 to $V_{DS,max}$ ranging from 1 to 12 V and then scanned back to 0, the forward and reverse scans retraced each other, demonstrating the reversible operation of the device within this V_{DS} range. However, when the scan range was increased to 14 V, we started to observe irreversible changes to the device. This can be illustrated by Figure 3b, which shows six consecutive I_{DS}−V_{DS} scans that were measured from 0 to $V_{DS,max}$ = 14 V and then back to 0. Figure 3b demonstrates that starting with the first I_{DS}−V_{DS} scan the reverse V_{DS} sweeps showed higher currents than the forward sweeps. The increased conductivity can be explained by the effect of current annealing, which is widely used to clean electronic devices based on other 2D materials, such as graphene, from adsorbed impurities by Joule heating and thus improve their transport characteristics.[31,32]

In the first scan in Figure 3b (see the brown I_{DS}−V_{DS} curve), as the drain−source voltage approached $V_{DS,max}$ = 14 V, the Joule heating became sufficient to improve the device conductivity, and as a result, in the reverse V_{DS} sweep the current was higher than in the forward sweep. Additional Joule heating could be performed by repeating the measurement. In the second forward V_{DS} sweep (see the dark orange curve in Figure 3b), the current coincides with the reverse sweep from the previous measurement, demonstrating that the conductivity improvement of the device is irreversible. Then, as the drain−source voltage approached $V_{DS,max}$ = 14 V again, the Joule heating further improved the conductivity, and the reverse sweep again showed a higher current than in the forward sweep. Consecutive I_{DS}−V_{DS} scans up to $V_{DS,max}$ = 14 V further annealed the device, resulting in a noticeable conductivity improvement with each measurement, see Figure 3b.

Further annealing could be performed by increasing the drain−source voltage scan range up to $V_{DS,max}$ = 15 V (Figure 3c) with the largest conductivity improvement observed in the first I_{DS}−V_{DS} scan. However, when the V_{DS} scan range was increased up to $V_{DS,max}$ = 16 V, the generated Joule heat became sufficiently high to cause irreversible damage to the device and resulted in a dramatic loss of current in the reverse sweep (Figure 3d). For convenience, all I_{DS}−V_{DS} scans from Figure 3a−d are plotted together in Figure 3e to demonstrate the gradual improvement of the device conductivity due to the

https://doi.org/10.1021/acsmaterialslett.1c00324
ACS Materials Lett. 2021, 3, 1088−1094

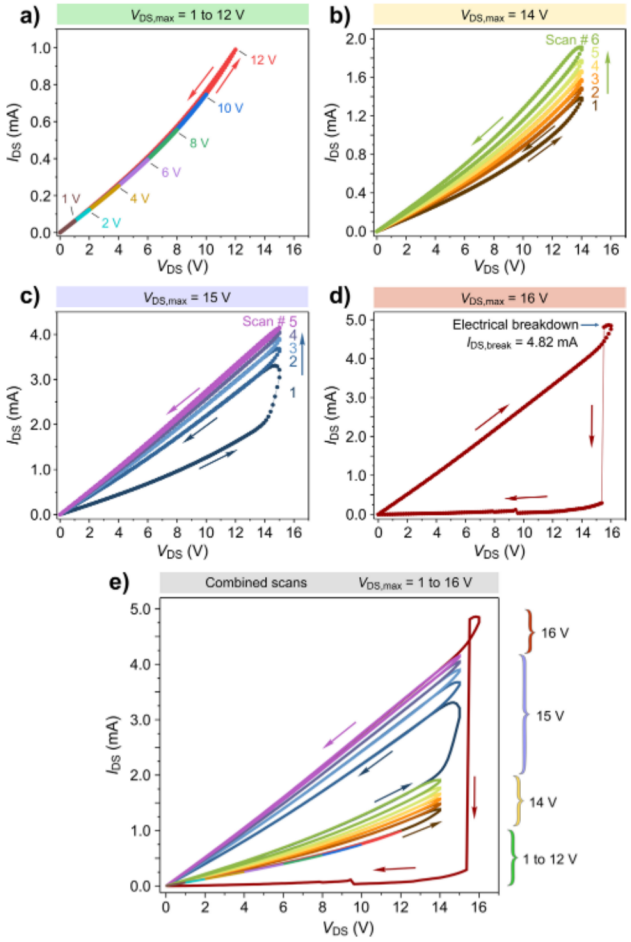

Figure 3. Stepwise current annealing and electrical breakdown of a monolayer $Nb_4C_3T_x$ flake. (a) Seven consecutive $I_{DS}-V_{DS}$ measurements of the same flake, in which the voltage was scanned from 0 up to $V_{DS,max}$ and then back to 0. In these measurements, $V_{DS,max}$ was consecutively increased from 1 to 12 V. (b) Six consecutive $I_{DS}-V_{DS}$ measurements, in which the voltage was scanned from 0 up to $V_{DS,max}$ = 14 V and then back to 0. (c) Five consecutive $I_{DS}-V_{DS}$ measurements, in which the voltage was scanned from 0 up to $V_{DS,max}$ = 15 V and then back to 0. (d) Electrical breakdown of the monolayer $Nb_4C_3T_x$ flake that occurred after the drain-source voltage was scanned from 0 to $V_{DS,max}$ = 16 V after the measurements shown in panels (a)−(c). (e) All $I_{DS}-V_{DS}$ curves from panels (a)−(d) shown in the same plot for clarity.

Joule heating until the electrical breakdown after the sweep up to $V_{DS,max}$ = 16 V.

The maximum current density of monolayer $Nb_4C_3T_x$ was calculated using the formula $j_c = I_{DS,max}/(wt)$, where $I_{DS,max}$ is the maximum I_{DS} measured before the breakdown, w is the average channel width, and t is the thickness (1.26 nm for the monolayer $Nb_4C_3T_x$).[25] For the tested monolayer $Nb_4C_3T_x$ devices, the average j_c is $1.05 \pm 0.11 \times 10^8$ A cm^{-2}. To put this value in context, we can compare this result with the breakdown current densities of other important electronic materials. The j_c value for $Nb_4C_3T_x$ is at least two orders of magnitude larger than the breakdown current density of copper, which is the most common interconnect material,[33−35] demonstrating the potential promise of $Nb_4C_3T_x$ MXene for interconnect applications. Compared to other 2D materials,

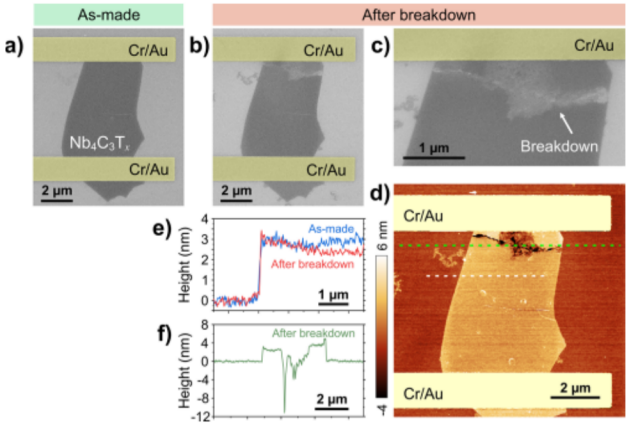

Figure 4. Effect of electrical breakdown on the morphology of a monolayer $Nb_4C_3T_x$ flake. (a) SEM image of a device based on a monolayer $Nb_4C_3T_x$ flake before the electrical testing. (b, c) SEM images of the same $Nb_4C_3T_x$ device after the electrical breakdown. Panel (c) shows the close-up view of the breakdown area. The Cr/Au contacts in panels (a)−(c) are highlighted in yellow for clarity. (d) AFM image of the same $Nb_4C_3T_x$ device after the electrical breakdown. The Cr/Au contacts are out of the range of the height scale bar. (e) AFM height profiles measured across the $Nb_4C_3T_x$ flake along the white dashed line in panel (d) before and after the electrical breakdown. (f) AFM height profile of the damaged area of the flake measured along the green dashed line in panel (d).

the breakdown current density of monolayer $Nb_4C_3T_x$ is much higher than for typical transition metal dichalcogenides, such as MoS_2 and WTe_2,[36,37] and is comparable to the materials with the highest j_c values on the order of 10^8 A cm^{-2}, including graphene,[33−35] $ZrTe_3$,[38] $TaSe_3$,[39−41] and single-walled carbon nanotubes.[42] Interestingly, the breakdown current density of $Nb_4C_3T_x$ is very close to that of $Ti_3C_2T_x$ MXene, which was recently reported to be $\sim 1.2 \times 10^8$ A cm^{-2}.[16] This observation suggests that a high breakdown current density is not an exclusive characteristic of $Ti_3C_2T_x$, but many other members of the large family of MXenes likely possess this property and could be employed in applications utilizing their high current-carrying capacity.

Figure 4 demonstrates the structural damage to monolayer $Nb_4C_3T_x$ due to the electrical breakdown. Figure 4a shows SEM image of a representative monolayer $Nb_4C_3T_x$ FET before the electrical characterization; the results of electrical measurements of this device are shown in Figure 3. After the $I_{DS}-V_{DS}$ scan up to $V_{DS,max}$ = 16 V, which resulted in the electrical breakdown (Figure 3d), this FET was imaged by SEM again, revealing a crack across the $Nb_4C_3T_x$ device channel, as shown in Figures 4b and 4c. Similar appearance of devices upon electrical breakdown was previously observed for $Ti_3C_2T_x$ MXene,[16] as well as other materials, such as amorphous carbon[43] and graphene.[34]

The changes to the $Nb_4C_3T_x$ device morphology due to the electrical breakdown were also investigated by AFM (Figure 4d). Figure 4e shows two AFM height profiles that were measured across the same area of the $Nb_4C_3T_x$ flake (see the white dashed line in Figure 4d) before and after the electrical breakdown. While the nominal thickness of monolayer $Nb_4C_3T_x$ can be estimated to be ~1.26 nm,[25] the measured AFM height of the as-prepared flake was ~2.9 nm (Figure 4e), which could be explained by the presence of molecular adsorbates, such as water molecules, trapped under the flake.

https://doi.org/10.1021/acsmaterialslett.1c00324
ACS Materials Lett. 2021, 3, 1088−1094